Ultrathin Nanosheets

International Edition: DOI: 10.1002/anie.201508939
German Edition: DOI: 10.1002/ange.201508939

Controllable Synthesis of Ultrathin Transition-Metal Hydroxide Nanosheets and their Extended Composite Nanostructures for Enhanced Catalytic Activity in the Heck Reaction

Hua Fan[+], Xing Huang[+], Lu Shang, Yitao Cao, Yufei Zhao, Li-Zhu Wu, Chen-Ho Tung, Yadong Yin, and Tierui Zhang**

Abstract: *We report an effective and universal approach for the preparation of ultrathin single- or multiple-component transition-metal hydroxide (TMH) nanosheets with thickness below 5 nm. The unique synthesis benefits from the gradual decomposition of the preformed metal–boron (M-B, M = Fe, Co, Ni, NiCo) composite nanospheres which facilitates the formation of ultrathin nanosheets by the oxidation of the metal and the simultaneous release of boron species. The high specific surface area of the sheets associated with their ultrathin nature promises a wide range of applications. For example, we demonstrate the remarkable adsorption ability of Pb^{II} and As^{V} in waste water by the ultrathin FeOOH nanosheets. More interestingly, the process can be extended simply to the synthesis of composite structures of metal alloy hollow shells encapsulated by TMH nanosheets, which show excellent catalytic activity in the Heck reaction.*

Two-dimensional (2D) transition-metal hydroxides (TMHs), particularly their ultrathin nanosheets with thickness of several nanometers, are attracting an increasing amount of attention[1] owing to their unique physical and chemical features, such as high specific surface areas, abundant active sites, and short diffusion path lengths for both ions and electrons.[2] These advantages make them better candidates, surpassing the physical capabilities of their bulk counterparts, or most of other nanostructures, especially for applications, such as energy storage,[3] catalysis,[4] and water treatment.[5] An excellent example was recently demonstrated by Xie et al., who showed that single-layer β-$Co(OH)_2$ sheets have a significantly enhanced specific capacitance (2028 $F g^{-1}$) compared to thicker sheets and bulk plates (525 $F g^{-1}$) because the single-layer sheets have more active sites and higher electrical conductivity.[2b]

Incommensurate with their high technical importance, the synthesis of TMH nanosheets has been limited mainly to hydrothermal and liquid exfoliation processes.[3b,6] While the hydrothermal approach usually involves harsh conditions, such as high temperature and lack of control over the thickness, exfoliation requires sophisticated procedures with relatively low yields. To address the synthetic challenge, herein, we report a simple, efficient, and versatile route for the large-scale synthesis of ultrathin nanosheets of TMHs (M = Fe, Co, Ni, NiCo) with typical thickness below 5 nm. The method is not only suitable for the synthesis of single- and multiple-component TMH ultrathin nanosheets, but also accessible for preparing hierarchical composites composed of metal alloy hollow spheres encapsulated by TMH nanosheets, such as PdNi@$Ni(OH)_2$. Intriguingly, the ultrathin FeOOH nanosheets exhibit a high adsorption capacity for Pb^{II} and As^{V}. As a catalyst in the Heck reaction, the PdNi@$Ni(OH)_2$ composite shows a high turnover number (TON) of approximately 3550000 and turnover frequency (TOF) of around 148000 h^{-1}.

This unique approach involves the preformation of metal–boron (M–B, M = Fe, Co, Ni) nanospheres and then their spontaneous transformation into ultrathin TMH nanosheets via a complete oxidation corrosion process in aqueous solutions. In a typical synthesis, a M^{II} salt was mixed with freshly prepared $NaBH_4$ solution in the presence of surfactant in deionized water, producing a black solution containing M–B nanospheres which then turned into ultrathin nanosheets upon exposure to air. Depending on the metal salt used, the products can be identified by X-ray diffraction (XRD, Figure 1 a–c) as δ-FeOOH (JCPDS 77-0247),[1b] α-$Co(OH)_2$ (JCPDS 46-0605),[7] and α-$Ni(OH)_2$ (JCPDS 38-0715).[4] The asymmetric nature of the reflections at 33.8° and 33.6° indicates the formation of the turbostratic α-$Co(OH)_2$ and α-$Ni(OH)_2$ (Figure 1 b,c).[7,8]

The representative scanning electron microscopy (SEM) images of the δ-FeOOH, α-$Co(OH)_2$, and α-$Ni(OH)_2$ all show three-dimensional frameworks consisting of highly flexible lamellar structures (Figure 1 d–f). The Energy-dispersive X-ray spectroscopy (EDX) spectra of the products (Figure 1, insets) further confirm their chemical composition. The thickness of these 2D nanosheets was determined by atomic force microscopy (AFM) to be as small as 1.8, 3.1, and 2.2 nm

[*] H. Fan,[+] Dr. X. Huang,[+] Dr. L. Shang, Y. Cao, Dr. Y. Zhao, Prof. L.-Z. Wu, Prof. C.-H. Tung, Prof. T. Zhang
Key Laboratory of Photochemical Conversion and Optoelectronic Materials, Technical Institute of Physics and Chemistry
Chinese Academy of Sciences
Beijing 100190 (P.R. China)
E-mail: tierui@mail.ipc.ac.cn
H. Fan,[+] Y. Cao
University of Chinese Academy of Sciences
Beijing 100049 (P.R. China)
Prof. Y. Yin
Department of Chemistry
University of California
Riverside, CA 92521 (USA)
E-mail: yadong.yin@ucr.edu
[+] These authors contributed equally to this work.

Supporting information for this article is available on the WWW under http://dx.doi.org/10.1002/anie.201508939.

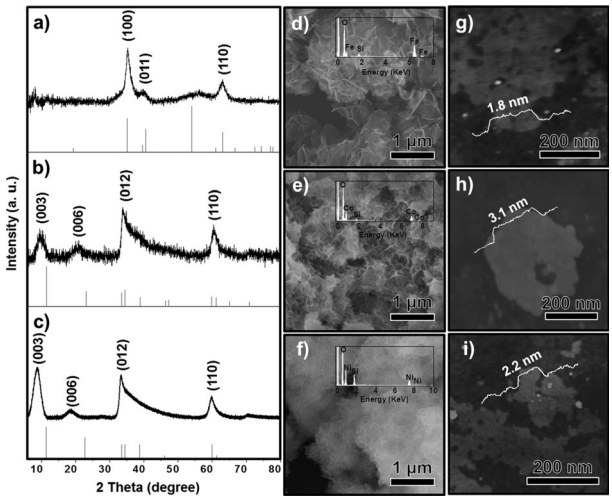

Figure 1. XRD patterns (left), SEM (middle), and AFM (right) images of the as-prepared a),d),g) FeOOH, b),e),h) $Co(OH)_2$, and c),f),i) $Ni(OH)_2$ ultrathin nanosheets. Insets are the corresponding EDX spectra.

for FeOOH, $Co(OH)_2$ and $Ni(OH)_2$, respectively (Figure 1 g–i). As expected from their small thicknesses, these TMH nanosheets possess large specific surface areas, showing 264, 184, and 442 $m^2 g^{-1}$ for FeOOH, $Co(OH)_2$, and $Ni(OH)_2$ nanosheets, respectively (Figure S1 in the Supporting Information), which to our knowledge are the highest values reported for corresponding TMHs.[9]

The morphology and structural information of the products were further revealed by transmission electron microscopy (TEM). As shown in Figure 2 a–c, these TMHs display

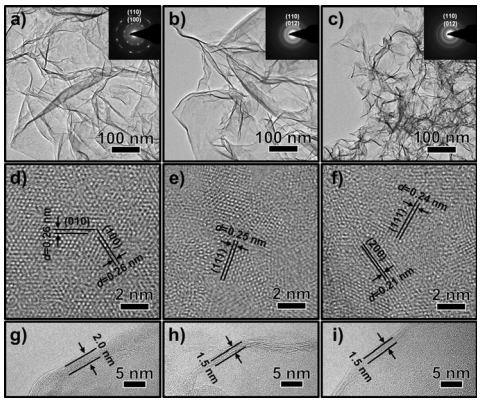

Figure 2. a)–c) TEM images of the TMH ultrathin nanosheets, insets show their corresponding SAED patterns; d)–f) HRTEM images of the nanosheets, indicating that $Co(OH)_2$ and $Ni(OH)_2$ can easily be transformed into CoO and NiO under beam irradiation; g)–i) HRTEM images taken from edges of the nanosheets.

a folding sheet-like morphology with lateral dimensions ranging from several hundred nanometers to several micrometers. The high transparency under the electron beam demonstrates their ultrathin nature. The insets in Figure 2 a–c show the corresponding selected-area electron diffraction (SAED) patterns. The line profiles derived from the diffraction patterns of $Co(OH)_2$ and $Ni(OH)_2$ show asymmetric peak intensity in the range of 3.7–3.8 nm^{-1}, further confirming the formation of turbostratic α-$Co(OH)_2$ and α-$Ni(OH)_2$ (Figure S2). The high resolution TEM (HRTEM) image of the FeOOH nanosheets shows hexagonal lattice fringes with a *d*-spacing of 0.26 nm, corresponding to the {100} planes of FeOOH (Figure 2 d). Because the α-$Co(OH)_2$ and α-$Ni(OH)_2$ were sensitive to electron beam irradiation (Figure S3), we were only able to catch HRTEM images of the CoO and NiO nanosheets evolved from the α-$Co(OH)_2$ and α-$Ni(OH)_2$ nanosheets (Figure 2 e,f). The thicknesses of the nanosheets determined from their edges (Figure 2 g–i) are approximately 1–2 nm, consistent with the AFM measurements.

To explore the growth mechanism of the ultrathin nanosheets, time course study was carried out on the nickel system. The initial black product from treating Ni^{II} with $NaBH_4$ consists of spherical particles with diameters of 60–80 nm (Figure 3 a), which are composed of small Ni crystallites (ca.

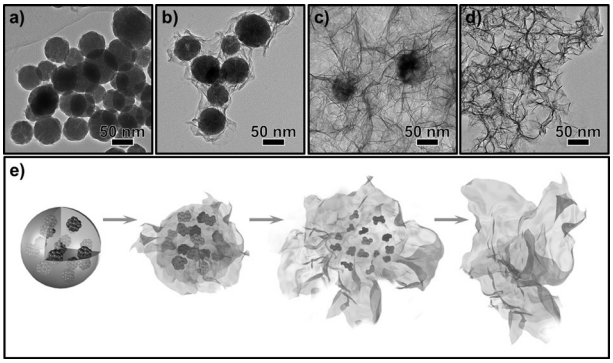

Figure 3. TEM images of Ni–B nanospheres a) before and b)–d) after exposure to the ambient atmosphere for b) 30 min, c) 8 h and d) 12 h; e) Schematic illustration of the formation of the ultrathin TMH nanosheets.

2 nm) embedded within an amorphous boron matrix as confirmed by the HRTEM and X-ray photoelectron spectroscopy (Figure S4), in line with a previous report.[10] The size and morphology of the Ni–B nanospheres remained almost unchanged with time. After the system was exposed to air for 30 min, $Ni(OH)_2$ nanosheets were observed around the nanospheres (Figure 3 b). The lateral dimension of the nanosheets increased remarkably with time, accompanied by the gradual disappearance of the nanospheres, producing only ultrathin $Ni(OH)_2$ nanosheets after 12 h (Figure 3 c,d). It can be clearly seen that the growth of $Ni(OH)_2$ nanosheets progressed at the expense of Ni–B nanospheres by the oxidation of Ni clusters in the Ni–B by ambient oxygen in the presence of water (Figure 3 e). This sequence was further demonstrated by the fact that the concentration of B in the solution increased gradually with the extension of exposure time (Figure S5). This result signifies that the oxidation of Ni occurred simultaneously with that of amorphous B which was then released into the solution, probably in the form of borate.[11] Thus, the gradual release of B from Ni–B spheres into solution enables the access of oxygen and water to the inside Ni nanoclusters, allowing their continued oxidation.

The formation of FeOOH and $Co(OH)_2$ nanosheets underwent a similar evolution process (Figure S6,7).

We believe that the unique Ni–B nanocomposite structure is crucial in this nanosphere-to-nanosheet transformation. In a parallel experiment involving pure Ni spheres instead of Ni–B spheres (Figure S8), only slight oxidation was found to occur on the surface of the Ni nanospheres even after four days, as the dense $Ni(OH)_2$ layer could prevent the further oxidation of Ni. While the intrinsic crystal structure of α-$Ni(OH)_2$ determines the preferred lateral growth of nanosheets, the adsorption of borate on the {001} facets of the nanosheets might contribute to the ultrathin characteristics by slowing down their axial growth.[2b]

This general process represents a new synthetic platform for developing various ultrathin 2D materials with a wide range of functionalities. For example, with their ultrahigh specific surface area as well as their large pore volume, the as-synthesized FeOOH nanosheets could be utilized as an efficient heavy-metal adsorbent for waste-water treatment. The room-temperature adsorption isotherms reveal that the maximum adsorption capacities of the FeOOH nanosheets for Pb^{II} and As^{V} are 114 and 109 $mg\,g^{-1}$, respectively (Figure S9). As far as we know, those values are the highest among reported Fe-based adsorbents (Table S1,2).[12]

This facile method can also be extended to the preparation of ultrathin multi-component TMH nanosheets by simply using mixed-metal precursors. In the example of Ni–Co hydroxide nanosheets shown in Figure S10, a homogeneous distribution of Ni, Co, and O elements throughout the entire sample was confirmed by the EDX elemental analysis. XRD measurement further demonstrates that the nanosheets are a single phase corresponding to Ni–Co layered double hydroxide.[13]

We further demonstrate that a simple modification to the M–B precursor could allow the fabrication of more complex nanocomposites. As the transition metals (Fe, Co, Ni) can easily form alloys with noble metals via Galvanic replacement and co-reduction,[14] M–B@NM (N = Au, Pt, Pd, and M = Fe, Co, Ni) core–shell structures could be readily synthesized and then transformed into interesting hierarchical hollow structures upon exposure to air. SEM and TEM images of the product obtained from the preformed Ni-B@PdNi show that it consists of hollow spheres fully covered by $Ni(OH)_2$ nanosheets (Figure 4a,b). The high-angle annular dark-field scanning TEM (HAADF-STEM) image (Figure 4c) clearly highlights the contrast between the hollow sphere and the enclosing $Ni(OH)_2$ nanosheets, with the higher contrast of the shells attributable to the presence of Pd, a heavier element. This result is confirmed by EDX elemental mapping analysis (Figure 4d–f,h). The enhancement of both Ni and Pd signals (Figure 4g) on the edge signifies the PdNi alloy shells. Further, as shown in the EDX line scan analysis in Figure 4i–k, the line profiles in three random edge positions show a similar trend in variation of the composition of Ni and Pd with a consistent O signal (O is from $Ni(OH)_2$), which again demonstrates the alloy nature of the shells. Additionally, the PdNi alloy was also analyzed by HRTEM (see Figure S11 and the corresponding discussion in the Supporting Information). This strategy is also applicable for the preparation of other hierarchical hollow structures, such as PtNi–$Ni(OH)_2$ (Figure S12).

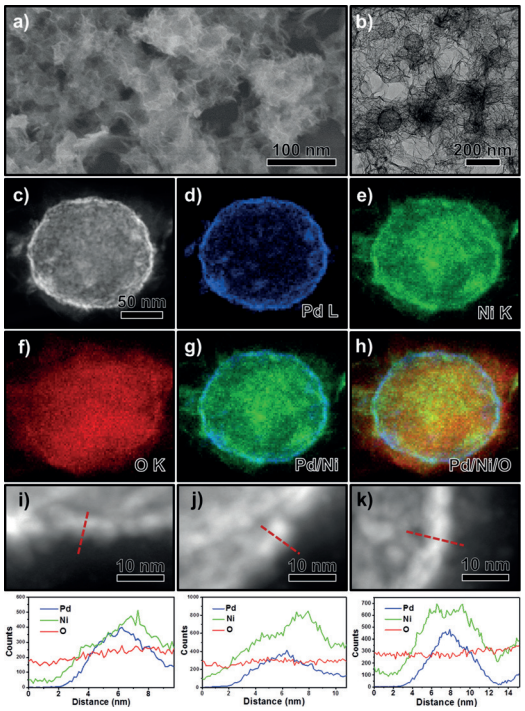

Figure 4. a) SEM and b) TEM images of the hierarchical hollow PdNi–$Ni(OH)_2$; c) HAADF-STEM image and d)–h) EDX mapping of PdNi–$Ni(OH)_2$; i)–k) EDX line scan in three random edge positions.

Palladium-catalyzed cross-coupling reactions are highly efficient paths for the creation of new C–C bonds.[15] As Pd is a precious metal with limited abundance, it is of great economic importance to lower its usage while maintaining the high activity.[16] As a demonstration, we used the hierarchical PdNi–$Ni(OH)_2$ as a catalyst in the Heck coupling reaction between iodobenzene and butyl acrylate (Scheme 1). After

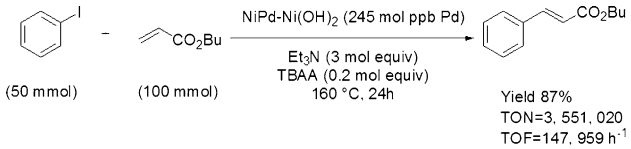

Scheme 1. Mizoroki–Heck reaction with the hierarchical PdNi–$Ni(OH)_2$ catalysts.

24 h, the desired butyl cinnamate was produced in a high yield of 87%. The corresponding TON and TOF were calculated to be as large as 3551020 and 147959 h^{-1}, respectively, which are far higher values than those reported previously (Table S3).[17] More interestingly, PdNi–$Ni(OH)_2$ also showed very stable catalytic activity during catalytic cycling tests (Figure S13). Although the exact mechanisms still require further exploration, we suspect that the high performance might come from the following aspects: 1) there is a "synergistic effect" between Ni and Pd in the alloy[16a] (Figure S14); 2) the

hollow shells composed of small-sized PdNi may ensure more accessible catalytic sites; 3) the high specific surface area $Ni(OH)_2$ as a support may stabilize the PdNi particles from leaching and aggregation during reaction (Table S4 and Figure S15).[18] With the simplicity of its synthesis and its excellent activity in the coupling reaction, the PdNi–$Ni(OH)_2$ catalyst is very promising for future practical utilization.

In summary, we have developed a simple, mild, and universal synthetic route to single- or multiple-component TMH nanosheets with thickness below 5 nm. Owing to the high specific surface area, the FeOOH nanosheets exhibited remarkable adsorption capacities for Pb^{II} and As^{V} of 114 and 109 $mg\,g^{-1}$, respectively. The unique synthesis benefits from the gradual decomposition of the preformed M–B nanocomposite spheres which facilitates the final formation of ultrathin nanosheets by the oxidation of M and the simultaneous release of boron species. More interestingly, we were able to extend the synthesis to the formation of hierarchical structures composed of metal alloy hollow shells covered with TMH nanosheets, which show excellent catalytic activity in the Heck reaction. We believe this process represents a new synthetic platform for developing various ultrathin 2D TMH materials for broad applications.

Acknowledgements

T.Z. thanks the financial support from the Ministry of Science and Technology of China (2014CB239402, 2013CB834505), the National Natural Science Foundation of China (51322213, 51172245, 91127005, 21401206, 21401207), and the Beijing Natural Science Foundation (2152033, 2154058). Y.Y. thanks the support from the U.S. Department of Energy (DE-SC0002247). X.H. thanks the instrument support from Fritz-Haber Institute of Max-Planck Society.

Keywords: Heck reaction · nanostructures · transition-metal hydroxides · two-dimensional materials · nanosheets

How to cite: *Angew. Chem. Int. Ed.* **2016**, *55*, 2167–2170
Angew. Chem. **2016**, *128*, 2207–2210

[1] a) R. Ma, T. Sasaki, *Acc. Chem. Res.* **2015**, *48*, 136–143; b) P. Z. Chen, K. Xu, X. L. Li, Y. Q. Guo, D. Zhou, J. Y. Zhao, X. J. Wu, C. Z. Wu, Y. Xie, *Chem. Sci.* **2014**, *5*, 2251–2255; c) Z. Gao, W. Yang, Y. Yan, J. Wang, J. Ma, X. Zhang, B. Xing, L. Liu, *Eur. J. Inorg. Chem.* **2013**, 4832–4838; d) R. Ma, K. Takada, K. Fukuda, N. Iyi, Y. Bando, T. Sasaki, *Angew. Chem. Int. Ed.* **2008**, *47*, 86–89; *Angew. Chem.* **2008**, *120*, 92–95; e) B. Ni, X. Wang, *Chem. Sci.* **2015**, *6*, 3572–3576.

[2] a) Y. Zhu, C. Cao, S. Tao, W. Chu, Z. Wu, Y. Li, *Sci. Rep.* **2014**, *4*, 5787; b) S. Gao, Y. Sun, F. Lei, L. Liang, J. Liu, W. Bi, B. Pan, Y. Xie, *Angew. Chem. Int. Ed.* **2014**, *53*, 12789–12793; *Angew. Chem.* **2014**, *126*, 13003–13007.

[3] a) Y. Zhao, Q. Wang, T. Bian, H. Yu, H. Fan, C. Zhou, L.-Z. Wu, C.-H. Tung, D. O'Hare, T. Zhang, *Nanoscale* **2015**, *7*, 7168–7173; b) L. Wang, C. Lin, F. Zhang, J. Jin, *ACS Nano* **2014**, *8*, 3724–3734.

[4] M. Gao, W. Sheng, Z. Zhuang, Q. Fang, S. Gu, J. Jiang, Y. Yan, *J. Am. Chem. Soc.* **2014**, *136*, 7077–7084.

[5] C. Peng, B. W. Jiang, Q. Liu, Z. Guo, Z. J. Xu, Q. Huang, H. J. Xu, R. Z. Tai, C. H. Fan, *Energy Environ. Sci.* **2011**, *4*, 2035–2040.

[6] a) S. Ida, D. Shiga, M. Koinuma, Y. Matsumoto, *J. Am. Chem. Soc.* **2008**, *130*, 14038–14039; b) H. Jiang, T. Zhao, C. Li, J. Ma, *J. Mater. Chem.* **2011**, *21*, 3818–3823.

[7] Z. Liu, R. Ma, M. Osada, K. Takada, T. Sasaki, *J. Am. Chem. Soc.* **2005**, *127*, 13869–13874.

[8] a) P. Jeevanandam, Y. Koltypin, A. Gedanken, *Nano Lett.* **2001**, *1*, 263–266; b) J. W. Lee, J. M. Ko, J.-D. Kim, *J. Phys. Chem. C* **2011**, *115*, 19445–19454.

[9] a) H. Li, W. Li, Y. Zhang, T. Wang, B. Wang, W. Xu, L. Jiang, W. Song, C. Shu, C. Wang, *J. Mater. Chem.* **2011**, *21*, 7878–7881; b) Y. Yao, C. Xu, S. Miao, H. Sun, S. Wang, *J. Colloid Interface Sci.* **2013**, *402*, 230–236; c) S.-I. Kim, P. Thiyagarajan, J.-H. Jang, *Nanoscale* **2014**, *6*, 11646–11652.

[10] J. Geng, D. A. Jefferson, B. F. G. Johnson, *Chem. Commun.* **2007**, 969–971.

[11] a) S. Carenco, D. Portehault, C. Boissière, N. Mézailles, C. Sanchez, *Chem. Rev.* **2013**, *113*, 7981–8065; b) J. Cueilleron, F. Thevenot, in *Boron and Refractory Borides* (Ed.: V. Matkovich), Springer, Berlin, Heidelberg, **1977**, pp. 203–213.

[12] a) B. Wang, H. Wu, L. Yu, R. Xu, T. T. Lim, X. W. Lou, *Adv. Mater.* **2012**, *24*, 1111–1116; b) S. Zeng, K. Tang, T. Li, Z. Liang, D. Wang, Y. Wang, W. Zhou, *J. Phys. Chem. C* **2007**, *111*, 10217–10225; c) X. Yu, S. Tong, M. Ge, J. Zuo, C. Cao, W. Song, *J. Mater. Chem. A* **2013**, *1*, 959–965; d) L. S. Zhong, J. S. Hu, H. P. Liang, A. M. Cao, W. G. Song, L. J. Wan, *Adv. Mater.* **2006**, *18*, 2426–2431.

[13] V. Gupta, S. Gupta, N. Miura, *J. Power Sources* **2008**, *175*, 680–685.

[14] Y. Vasquez, A. K. Sra, R. E. Schaak, *J. Am. Chem. Soc.* **2005**, *127*, 12504–12505.

[15] X.-F. Wu, P. Anbarasan, H. Neumann, M. Beller, *Angew. Chem. Int. Ed.* **2010**, *49*, 9047–9050; *Angew. Chem.* **2010**, *122*, 9231–9234.

[16] a) R. K. Rai, K. Gupta, S. Behrens, J. Li, Q. Xu, S. K. Singh, *ChemCatChem* **2015**, *7*, 1806–1812; b) Y. Wu, D. Wang, P. Zhao, Z. Niu, Q. Peng, Y. Li, *Inorg. Chem.* **2011**, *50*, 2046–2048.

[17] a) Y. M. A. Yamada, Y. Yuyama, T. Sato, S. Fujikawa, Y. Uozumi, *Angew. Chem. Int. Ed.* **2014**, *53*, 127–131; *Angew. Chem.* **2014**, *126*, 131–135; b) J.-N. Young, T.-C. Chang, S.-C. Tsai, L. Yang, S. J. Yu, *J. Catal.* **2010**, *272*, 253–261; c) H. Hagiwara, Y. Sugawara, K. Isobe, T. Hoshi, T. Suzuki, *Org. Lett.* **2004**, *6*, 2325–2328; d) K. Okamoto, R. Akiyama, H. Yoshida, T. Yoshida, S. Kobayashi, *J. Am. Chem. Soc.* **2005**, *127*, 2125–2135.

[18] P. Li, P.-P. Huang, F.-F. Wei, Y.-B. Sun, C.-Y. Cao, W.-G. Song, *J. Mater. Chem. A* **2014**, *2*, 12739–12745.

Received: September 29, 2015
Published online: December 3, 2015

